PHOTONICS Research

Polarization-robust mid-infrared carpet cloak with minimized lateral shift

Yao Huang,[1] Jingjing Zhang,[2,7] Jinhui Zhou,[3] Bo Qiang,[1] Zhengji Xu,[4] Lin Liu,[1] Jifang Tao,[5] Nicolas Kossowski,[1] Qijie Wang,[1,6,8] and Yu Luo[1,9]

[1]School of Electrical and Electronic Engineering, Nanyang Technological University, Singapore 639798, Singapore
[2]State Key Laboratory of Millimeter Waves, Southeast University, Nanjing 210096, China
[3]Electrical Engineering, Kulicke & Soffa Pte. Ltd., Singapore 554369, Singapore
[4]School of Microelectronics Science and Technology, Sun Yat-sen University, Zhuhai 519082, China
[5]School of Information and Engineering, Shandong University, Qingdao 266237, China
[6]School of Physical and Mathematical Sciences, Nanyang Technological University, Singapore 637371, Singapore
[7]e-mail: zhangjingjing@seu.edu.cn
[8]e-mail: qjwang@ntu.edu.sg
[9]e-mail: luoyu@ntu.edu.sg

Received 12 November 2020; revised 24 February 2021; accepted 4 March 2021; posted 25 March 2021 (Doc. ID 414437); published 20 May 2021

With the advent and rapid development of the transformation optics and metamaterials, invisibility cloaks have captivated much attention in recent years. While most cloaking schemes suffer from limited bandwidth, the carpet cloak, which can hide an object on a reflecting plane, can operate over a broadband frequency range. However, the carpet cloaks experimentally realized thus far still have several limitations. For example, the quasi-conformal mapping carpet cloak leads to a lateral shift of the reflected light ray, while the birefringent carpet cloak only works for a specific polarization. In this work, we propose a conformal transformation scheme to tackle these two problems simultaneously. As an example, we design a mid-infrared carpet cloak in a silicon platform and demonstrate its polarization-insensitive property as well as the minimized lateral shift over a broad frequency band from 24 to 28.3 THz.

https://doi.org/10.1364/PRJ.414437

1. INTRODUCTION

Invisibility cloaks, originally existing in scientific fiction and movies, have attracted people's interest for centuries. For military applications, they can be used as stealth coating to conceal tanks, aircrafts, submarines, and so on. For commercial applications, they can be used to prevent unwanted scattering from defects in antennas, lasers, electronic circuits, and so on. The recent development of transformation optics and metamaterials greatly promotes the experimental realization of cloaking devices [1–10]. As theoretically demonstrated by Pendry and coworkers in 2006, ideal invisibility cloaks in free space generally require near-zero permittivity/permeability components. Although several types of such cloaks have been experimentally implemented in the microwave regime [11,12], the resonant elements involved (to realize near-zero permittivity or permeability) greatly limit their bandwidths. To tackle this problem, Li and Pendry proposed the concept of a "carpet" cloak, which, instead of transparentizing the hidden object, makes it reflect light as a flat surface [13]. Since carpet cloaks no longer require near-zero value in permittivity or permeability, they have the intrinsic advantages of lower dissipation loss and broader working bandwidth as compared with free-space cloaks [13]. Under optical surface transformation, the optic-null medium helps to build a wide-illumination range and low-loss invisibility cloak, while it only works under TM polarization [14].

In general, carpet cloaks can be designed using either quasi-conformal mapping or bilinear transformation [15]. Earlier experimental realizations of carpet cloaks are generally based on quasi-conformal mappings [16–19]. This type of carpet cloaks operates on inhomogeneous refractive index and works for unpolarized light as demonstrated at both microwave [20] and optical frequencies [21]. However, the approximation made in quasi-conformal mapping leads to a lateral shift of the reflected light beam, whose value is comparable to the dimension of the hidden object, and hence makes the object detectable [22]. On the other hand, carpet cloaks designed with bilinear transformation make use of several birefringent crystals judiciously glued together [23,24]. This type of cloak eliminates the lateral shift, but it only works for a specific light polarization. Recently, with the advent of metasurfaces, an ultrathin carpet cloak design was proposed. By judiciously designing the meta-atoms to achieve the required phase shift and restore the phase front, the full-polarization metasurface-based skin cloak has been realized

[25]. In addition, the tunable metasurface illusion device can be constructed by applying programmable voltage source to adjust the varactor configurations on the metasurface [26]. However, these metasurface cloak designs have limited working bandwidths. Up to now, the design and implementation of a broadband carpet cloak that is polarization insensitive while addressing the problem of lateral shift are still challenging.

In this paper, we attempt to tackle the two problems mentioned above simultaneously. We target at mid-infrared (IR) frequency range, owing to its wide application in military and industry, such as semiconductor processing, spectroscopy, chemical and biomolecular sensing, and security. Many mid-IR devices have been proposed and implemented, including lasers [27,28], sensors [29,30], and frequency combs [31]. However, to the best of our knowledge, an invisibility cloak has never been realized in this frequency range [32–40]. Our approach makes use of a judiciously designed conformal mapping, and the resultant carpet cloak relies only on an isotropic nonresonant medium. Moreover, our carpet cloak design is based on commercially available silicon-on-insulator (SOI) wafers and is suitable for mass production of on-chip cloaking devices.

2. RESULTS AND DISCUSSION

The proposed cloaking device fills the region between the black solid straight line and the continuous wavy curve shown in Fig. 1. Through a conformal transformation

$$x' = \frac{1}{2}\ln\left\{\frac{e^{2x}\cos^2 y + [be^{2x} - (2ab+1)e^{x}\sin y + a^2 b + a]^2}{(e^{2x} - 2a\sin y + a^2)^2}\right\}, \tag{1}$$

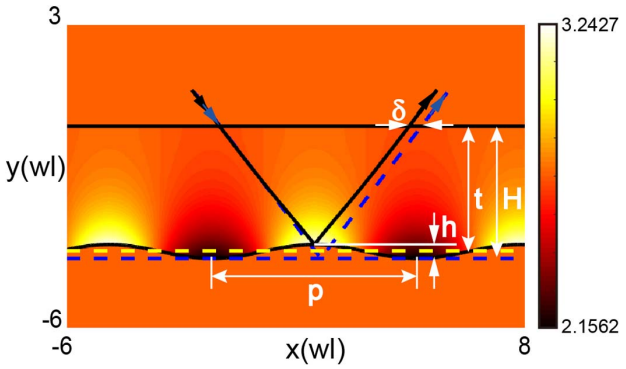

Fig. 1. Light ray tracing for a conformal carpet cloak with minimized lateral shift. The carpet cloak covers the top of a curved PEC bump, making it reflect light as a virtual flat plane denoted by the blue dashed line. The blue and black solid arrows indicate the trajectories of light reflected by the virtual plane and the cloak, respectively. The contour plot represents the refractive index distribution for the cloak. The cloak is designed with a conformal transformation with $a = 0.005$, $b = 0.005$, and $t = 3.7$.

$$y' = \arctan\left[\frac{be^{2x} - (2ab+1)e^{x}\sin y + a^2 b + a}{e^{x}\cos y}\right], \tag{2}$$

the cloak region is mapped into a planar slab (with a thickness t) sandwiched between the black solid straight line and the yellow dashed straight line in Fig. 1. Under such a conformal mapping, a planar surface (as indicated by the yellow dashed line) is transformed to bumps (as indicated by the wavy curve) with periodicity p [41]. If the transformed slab has a constant refractive index n_0, the cloak region will acquire a spatially gradient isotropic refractive index given by

$$n' = n_0 \frac{|e^{x'}|}{\sqrt{(e^{2x'} - 2be^{x'}\sin x' + b^2)[a^2 e^{2x'} - 2(1+ab)ae^{x'}\sin x' + (1+ab)^2]}}. \tag{3}$$

According to the theory of transformation optics, light reflected from the bump surface covered with the cloak will propagate in exactly the same way as the reflected beam from a planar surface. The transformation parameters a, b, and t control the shape of the bumps (e.g., height of bumps h) as well as the range of refractive indices of the cloak (e.g., minimum and maximum values of refractive indices) according to

$$h = \ln\left\{\frac{[be^{2x_0} - (2ab+1)e^{-x_0} + a^2 b + a](e^{2x_0} + 2a + a^2)}{[be^{2x_0} + (2ab+1)e^{-x_0} + a^2 b + a](e^{2x_0} - 2a + a^2)}\right\}, \tag{4}$$

$$n_{\min} = n_0 \frac{\sqrt{(e^{2x_0} - 2ae^{x_0} + a^2)[b^2 e^{2x_0} - 2(1+ab)be^{x_0} + (1+ab)^2]}}{|e^{x_0}|}, \tag{5}$$

$$n_{\max} = n_0 \frac{\sqrt{(e^{2x_0} + 2ae^{x_0} + a^2)[b^2 e^{2x_0} + 2(1+ab)be^{x_0} + (1+ab)^2]}}{|e^{x_0}|}, \tag{6}$$

where

$$x_0 = \frac{1}{2}\ln\left(a^2 + \frac{a}{b}\right) - t. \tag{7}$$

In principle, a, b, and t can be arbitrary positive values but must be judiciously designed in order to make the implementation of the cloak experimentally feasible. In our design, these parameters are chosen as $a = 0.005$, $b = 0.005$, and $t = 3.7$ to hide $0.41\lambda_0$ high bumps in a background with a refractive index $n_0 = 2.7$. The corresponding refractive indices of the cloak range from 2.1562 to 3.2427. As depicted by the contour plot in Fig. 1, the minimum and the maximum refractive indices occur at the valleys and the peaks of the bumps, respectively. Away from the bumps, the cloak index gradually changes

to n_0 (i.e., he background index), fulfilling the condition of impedance match.

We analytically retrieve and compare the light trajectories in the systems of a cloak and a virtual slab as shown in Fig. 1. In the cloak system, the ray position vector is obtained by solving a differential eikonal equation [42]

$$\frac{\mathrm{d}}{\mathrm{d}s}\left[n(\mathbf{r})\frac{\mathrm{d}r}{\mathrm{d}s}\right] = \nabla n(\mathbf{r}), \tag{8}$$

where $\mathbf{r}$ is the ray position vector, $n(\mathbf{r})$ is the index of refraction, and s is an incremental path distance. For arbitrary $n(\mathbf{r})$, [Eq. (8)] can be solved numerically, e.g., through a graphic iterative method [43]. In our case, the refractive index of the cloak takes the form of Eq. (3), and the analytical solution of the ray position vector $\mathbf{r}$ can be obtained.

In the system of a virtual slab, the reflecting plane denoted by the blue dashed line is located at the bottom of the cloak. The thickness of this virtual slab equals the height of the cloak indicated by H. The ray diagram presented in Fig. 1 clearly shows the lateral shift δ between the reflected light ray from the cloaked bumps and that from a flat perfect electric conductor (PEC) plane [44–46]. The lateral shift δ results from the nonzero value of $H - t$, i.e., height difference between the equivalent reflection plane of the cloak (yellow dashed plane) and the virtual reflection plane of the slab (blue dashed plane). Mathematically, δ takes the following form:

$$\delta = 2(H - t)\tan\theta, \tag{9}$$

where θ is the incident angle.

Our conformal mapping approach provides a quantitative method to calculate and minimize the lateral shift. According to Eq. (9), reducing the distance $H - t$ is the most straightforward way to minimize the lateral shift. This distance is controlled by geometric parameters including periodicity (p) and cloak height (H). Therefore, we analytically calculate the lateral shift variance in terms of the periodicity (p) and cloak height (H) in Figs. 2(a) and 2(b), respectively, and here the lateral shift is defined as δ/h. As shown in Fig. 2(a), when the periodicity increases from 2.55 to 7.14, the lateral shift δ/h first decreases from 0.61 to 0.52 and then gradually increases to 0.54. The smallest lateral shift 0.52 appears at periodicity $p = 30.1$. This indicates that a proper choice of periodicity can effectively reduce the lateral shift. However, the enlarged periodicity also induces the increased refractive index variation along the interface between the free space and the cloak. This growing variation results in the increased reflection at the upper boundary of the cloak under both TE and TM polarizations as presented by the two blue curves in Fig. 2(a). The reflection R is simulated through COMSOL according to $R = T_0 - T_1$, where T_1 is the transmission of the interface indicated by the black straight line (in Fig. 1) in the cloak system and T_0 is the transmission in free space as a reference. Therefore, the trade-off between the lateral shift and the reflection needs to be considered in the design. As depicted in Fig. 2(b), it is worth noticing that the height of the cloak (H) has no influence on the lateral shift. Meanwhile, with cloak height growing from 3.34 to 5.89, the reflection decreases. This indicates that increasing the cloak height enables the reduction of reflection without affecting the lateral shift. Thus, a proper periodicity and a large cloak height will offer a balance between the lateral shift minimization and reflection reduction regardless of the polarization. Furthermore, the red symbols in Fig. 2 denote the lateral shift and reflection with geometric parameters applied in Fig. 1, corresponding to the optimized performance for both polarizations for the mid-IR implementation.

To further demonstrate its polarization-robust property, we conduct finite element simulations through COMSOL to evaluate the performance of our cloak. We simulate and compare the field distributions for two different scenarios: 1) the reflection from bare PEC bumps illuminated by a Gaussian beam launched 32° with respect to the horizontal direction and 2) the reflection from the cloaked PEC bumps under the same illumination. The designed carpet cloak filling the region between the black straight line and the wavy curve in Figs. 3(b) and 3(d) has a refractive index distribution given by Eq. (3). For simplicity but without loss of generality, the working wavelength is normalized to $\lambda = 1$. In Figs. 3(a) and 3(b), the incident Gaussian beam is polarized along the TE direction. Apparently, the beam illuminating bare PEC bumps is scattered into various directions as shown in Fig. 3(a). Strong scattering is observed from the distorted wavefront of the reflected beam. On the contrary, covering the bumped surface with the proposed carpet cloak greatly suppressed the wavefront distortion as depicted in Fig. 3(b). Moreover, with the presence of the cloak, the wavefront of the reflected beam remains the same as if reflected by a flat ground plane. It is also worth noticing that no scattering is observed at the interface of the background and the cloak because of the matched

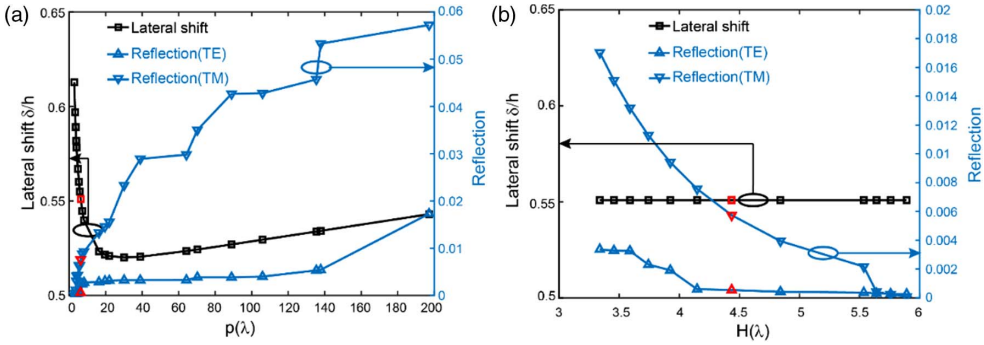

Fig. 2. Minimization of the lateral shift. Analytically calculated lateral shift and simulated reflection coefficients (for TE and TM polarizations) at the interface between the background and the cloak as a function of (a) the periodicity p and (b) the cloak height H.

impedance at this boundary. This feature results from the reasonable choice of transformation parameters, which make the refractive index continuous across this interface. Furthermore, we also simulate and compare the field distributions for uncloaked and cloaked bump with the Gaussian beam launched 42° with respect to the horizontal direction in Figs. 3(c) and 3(d), respectively. The robust cloaking performance under larger incident angle is clearly demonstrated.

To test the cloak performance for TM polarization, we plot the magnetic field distributions in Figs. 3(e)–3(h) when the polarization of the incident Gaussian beam is switched to TM. As expected, the scattering produced by the bumped surface in Figs. 3(e) and 3(g) is eliminated by the carpet cloak in Figs. 3(f) and 3(h), respectively. Considering the generality of our conformal transformation approach, this minimized lateral shift polarization-robust carpet cloak can be implemented in any frequency range with a proper choice of the material.

Based on the above theoretical study, we propose here a practical implementation of this carpet cloak in the mid-IR as an example. The working wavelength is targeted at $\lambda = 10.6$ μm. The blueprint of the mid-IR carpet cloak is displayed in Fig. 4(a), where the dimensions of the cloak are 48 μm in length, 19.63 μm in width, and 2.05 μm in bump height. The cloak is constructed on an SOI wafer with a 2 μm thick silicon device layer separated by a 5 μm thick silicon dioxide box layer from the silicon substrate as depicted in the inset of Fig. 4(a). Light is confined in the 2 μm thick silicon device layer and propagates only along the in-plane directions. Considering the thickness of the silicon device layer, only the fundamental mode exists in the planar SOI waveguide around 10 μm. Its propagation constant follows the equation

$$k_{\parallel} = \sqrt{n_{\text{silicon}}^2 \left(\frac{2\pi}{\lambda}\right)^2 - k_z^2}, \tag{10}$$

where n_{silicon} is the refractive index of silicon. The effective refractive index of the SOI waveguide mode can be obtained using the following equation:

$$n_{\text{eff}} = \sqrt{n_{\text{silicon}}^2 - \left(\frac{k_z \lambda}{\pi}\right)^2}. \tag{11}$$

The required refractive index distribution of the cloak can be realized by drilling subwavelength holes with different radii into the silicon device layer at a fixed periodicity. As mentioned before, the refractive index of the background medium in our design is set as $n = 2.7$, and the refractive index distributions of the cloak span from 2.1562 to 3.2427 as shown in Fig. 1. We use the following equation to deduce the hole radius distribution for the whole device:

$$R(w) = p\sqrt{\frac{(n' n_0)^2 - n_{\text{eff}}^2}{\pi(n_{\text{eff}}^2 - 1)}}, \tag{12}$$

where $R(w)$ is the hole radius, p is the periodicity of the holes, and n' is the refractive index distribution of the cloak. When the periodicity of the holes is fixed at $p = 1.5$ μm, such a refractive index distribution can be realized by varying the hole radius from 75 to 1300 nm.

The commercial software CST Microwave Studio is used to examine the performance of the cloak implemented on the SOI wafer. The refractive indices of silicon and silica are taken from Ref. [47] and Ref. [48], respectively. Figures 4(b) and 4(c) plot

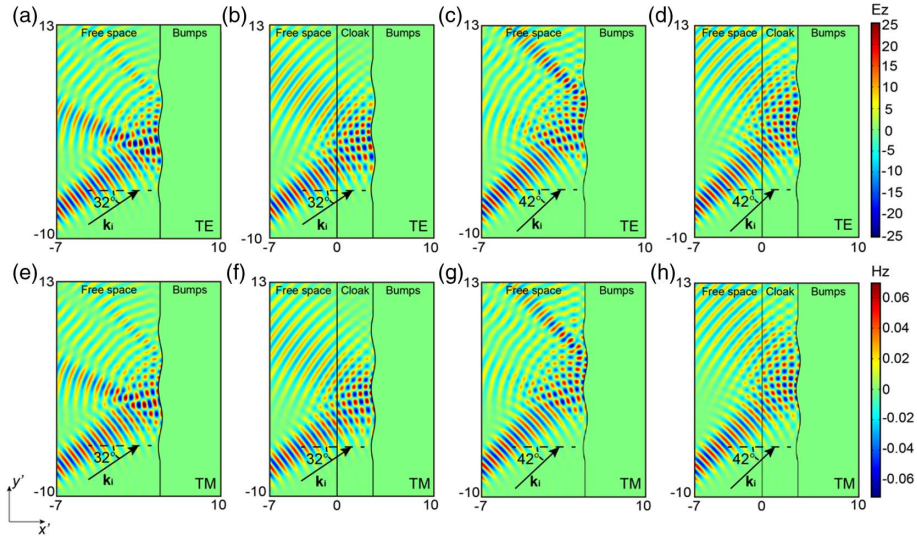

Fig. 3. Numerical verification of the polarization-insensitive performance. Simulated electric field distributions of a bumped surface (a) without the cloak and (b) with the cloak when a TE-polarized Gaussian beam is incident at an angle 32° with respect to the horizontal direction. Simulated electric field distributions of a bumped surface (c) without the cloak and (d) with the cloak when a TE-polarized Gaussian beam is incident at an angle 42° with respect to the horizontal direction. Simulated magnetic field distributions of a bumped surface (e) without the cloak and (f) with the cloak when a TM-polarized Gaussian beam is incident at an angle 32° with respect to the horizontal direction. Simulated magnetic field distributions of a bumped surface (g) without the cloak and (h) with the cloak when a TM-polarized Gaussian beam is incident at an angle 42° with respect to the horizontal direction.

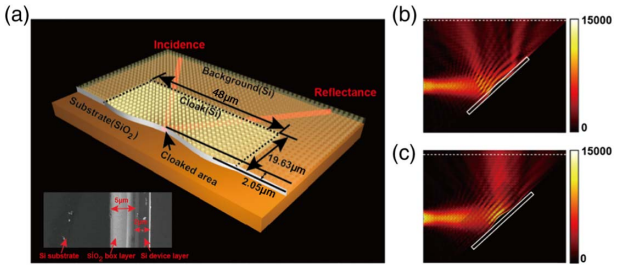

Fig. 4. Blueprint of the mid-IR carpet cloak designed at a wavelength $\lambda = 10.6$ μm. (a) Schematic of the practical implementation of the cloak. Light is incident upon a triangular background drilled with homogenous holes. The cloak is built by drilling spatially gradient holes into an SOI wafer. Magnetic field distributions when a TM-polarized Gaussian beam is incident at an angle 45° onto (b) a bare bump and (c) a bumped surface covered with the cloak.

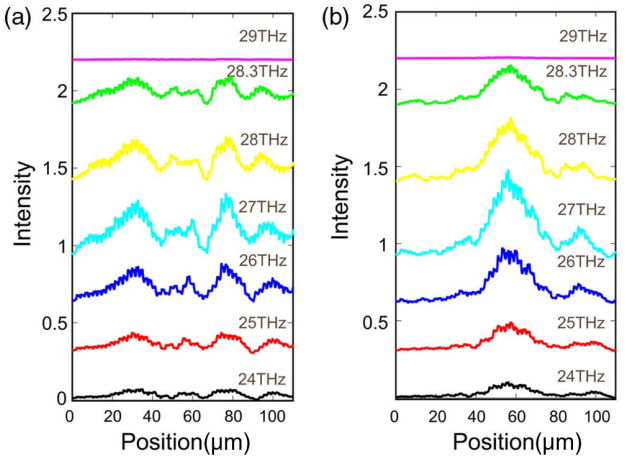

Fig. 5. Demonstration of the robust cloaking performance over a broad frequency range from 24 to 29 THz. (a) Intensity profile versus the different positions along the white dashed line in Fig. 4(b) when the incident laser beam illuminates the bare bump. (b) Intensity profile versus the different positions along the white dashed line in Fig. 4(c) when the incident laser beam illuminates the bump covered with the cloak.

the magnetic field intensities at the top plane of the silicon device layer when a Gaussian beam is incident upon (1) a bare bump and (2) a bump surface covered by the cloak. Through the comparison, we can observe remarkable scattering from the bare bump, whereas such scattering is dramatically suppressed by the presence of the cloak, giving rise to a single reflection profile. In other words, the cloak has successfully concealed the curved bump, making it reflect light as a flat PEC plane. Moreover, the suppressed scattering is observed for arbitrary incident angles, verifying the excellent performance of the cloak implemented on the SOI wafer. Since light will never penetrate into the PEC bump, any object could be hidden behind the bump and appear invisible to the observers outside.

Since resonant elements are avoided in our design, the SOI cloak is expected to work over a broad frequency band. In order to further demonstrate the broadband cloaking performance, we simulate the intensity profiles of the reflection beams [i.e., along the white dashed line in Figs. 4(b) and 4(c)] at seven different frequencies from 24 to 29 THz, with the commercial software, CST Microwave Studio. Results for bare and cloaked bumps are presented in Figs. 5(a) and 5(b), respectively. The x axis indicates the different positions on the white dashed line in Figs. 4(b) and 4(c). The positions 0 and 110 μm in Figs. 5(a) and 5(b) correspond to left and right ends of the white dashed line. As shown in Fig. 5(a), the reflection intensity profile of the bare bump presents several distinct peaks at all seven frequencies, illustrating the significant deflections brought by the uneven reflection surface. Unlike the bare bump, within the frequency band ranging from 24 to 28.3 THz, the beam profile shows a single peak along the output position as depicted in Fig. 5(b), indicating that the deflection from the curved bump is dramatically suppressed by the presence of the cloak. These results imply that our SOI cloak has successfully redirected the light propagation and presented the external observers an illusion of a flat reflective surface. Any object hidden underneath the wavy bump will never be perceived. Moreover, results in Fig. 5(b) clearly demonstrate that the cloaking performance is robust against frequency change within 24 to 28.3 THz. The intensity of the reflection beam at 29 THz is much weaker than that at other frequencies, owing to the strong chromatic dispersion of the silicon dioxide substrate at high frequencies, e.g., the chromatic dispersion effect reduces the refractive index contrast between the silicon and the silicon dioxide layer toward high frequencies, making the confinement of the light in the silicon device layer much weaker above 29 THz.

3. CONCLUSION

In conclusion, we propose a mid-IR carpet cloak based on a judiciously designed conformal transformation. This cloak operates on isotropic refractive index, which can be easily implemented with nonresonant structures. Analytical calculations and numerical simulations show that through properly choosing the periodicity p and increasing the cloak height H, the lateral shift can be effectively minimized with the reflection controlled. The polarization-robust performance over a broadband frequency range is also demonstrated. The practical implementation of this cloak can be realized on the platform of commercially available SOI wafers by drilling spatially gradient holes with judiciously designed radii into the silicon layer. Our conformal transformation approach not only provides an alternative solution for cloak design but also offers a general platform for the design of other optical devices such as lenses, waveguides, and optical cavities.

Funding. Ministry of Education - Singapore (MOE 2018-T2-2-189 (S), MOE2018-T2-1-176); National Research Foundation Singapore (NRF-CRP18-2017-02, NRF-CRP22-2019-0006); Agency for Science, Technology and Research (A18A7b0058, A20E5c0095); National Natural Science Foundation of China (61871127).

Disclosures. The authors declare no conflicts of interest.

REFERENCES

1. A. J. Ward and J. B. Pendry, "Refraction and geometry in Maxwell's equations," J. Mod. Opt. **43**, 773–793 (1996).

2. U. Leonhardt, "Optical conformal mapping," Science **312**, 1777–1780 (2006).
3. H. Chen, B. I. Wu, B. Zhang, and J. A. Kong, "Electromagnetic wave interactions with a metamaterial cloak," Phys. Rev. Lett. **99**, 063903 (2007).
4. H. Chen, C. T. Chan, and P. Sheng, "Transformation optics and metamaterials," Nat. Mater. **9**, 387–396 (2010).
5. Y. Liu and X. Zhang, "Recent advances in transformation optics," Nanoscale **4**, 5277–5292 (2012).
6. T. Han, X. Bai, D. Gao, J. T. L. Thong, B. Li, and C. W. Qiu, "Experimental demonstration of a bilayer thermal cloak," Phys. Rev. Lett. **112**, 054302 (2014).
7. J. Y. H. Teo, L. J. Wong, M. C. Molardi, and P. Genevet, "Controlling electromagnetic fields at boundaries of arbitrary geometries," Phys. Rev. A **94**, 023820 (2016).
8. H. Chu, Q. Li, B. Liu, J. Luo, S. Sun, Z. H. Hang, L. Zhou, and Y. Lai, "A hybrid invisibility cloak based on integration of transparent metasurfaces and zero-index materials," Light Sci. Appl. **7**, 50 (2018).
9. J. Zhang, J. B. Pendry, and Y. Luo, "Transformation optics from macroscopic to nanoscale regimes: a review," Adv. Photon. **1**, 014001 (2019).
10. E. Bor, U. G. Yasa, H. Kurt, and M. Turduev, "Demonstration of carpet cloaking by an anisotropic zero refractive index medium," Opt. Lett. **45**, 2423–2426 (2020).
11. J. B. Pendry, D. Schurig, and D. R. Smith, "Controlling electromagnetic fields," Science **312**, 1780–1782 (2006).
12. D. Schurig, J. J. Mock, B. J. Justice, S. A. Cummer, J. B. Pendry, A. F. Starr, and D. R. Smith, "Metamaterial electromagnetic cloak at microwave frequencies," Science **314**, 977–980 (2006).
13. J. Li and J. B. Pendry, "Hiding under the carpet: a new strategy for cloaking," Phys. Rev. Lett. **101**, 203901 (2008).
14. F. Sun, Y. Zhang, J. Evans, and S. He, "A camouflage device without metamaterials," Prog. Electromagn. Res. **165**, 107–117 (2019).
15. F. Liu, J. Li, J. Zhang, and Y. Luo, *World Scientific Handbook of Metamaterials and Plasmonics* (World Scientific, 2017), Vol. **2**, Chap.11.
16. J. Valentine, J. Li, T. Zentgraf, G. Bartal, and X. Zhang, "An optical cloak made of dielectrics," Nat. Mater. **8**, 568–571 (2009).
17. T. Ergin, N. Stenger, P. Brenner, J. B. Pendry, and M. Wegener, "Three-dimensional invisibility cloak at optical wavelengths," Science **328**, 337–339 (2010).
18. T. Ergin, J. Fischer, and M. Wegener, "Detailed optical characterization of three-dimensional visible-frequency polarization-independent carpet invisibility cloak," Phys. B Condens. Matter **407**, 4075–4077 (2012).
19. N. Wang, Y. Ma, R. Huang, and C. K. Ong, "Far field free-space measurement of three dimensional hole-in-teflon invisibility cloak," Opt. Express **21**, 5941–5948 (2013).
20. H. F. Ma and T. J. Cui, "Three-dimensional broadband ground-plane cloak made of metamaterials," Nat. Commun. **1**, 21 (2010).
21. M. Gharghi, C. Gladden, T. Zentgraf, Y. Liu, X. Yin, J. Valentine, and X. Zhang, "A carpet cloak for visible light," Nano Lett. **11**, 2825–2828 (2011).
22. B. Zhang, T. Chan, and B.-I. Wu, "Lateral shift makes a ground-plane cloak detectable," Phys. Rev. Lett. **104**, 233903 (2010).
23. X. Chen, Y. Luo, J. Zhang, K. Jiang, J. B. Pendry, and S. Zhang, "Macroscopic invisibility cloaking of visible light," Nat. Commun. **2**, 176 (2011).
24. D. C. Liang, J. Q. Gu, J. G. Han, Y. M. Yang, S. Zhang, and W. L. Zhang, "Robust large dimension terahertz cloaking," Adv. Mater. **24**, 916–921 (2012).
25. Y. Yang, L. Jing, B. Zheng, R. Hao, W. Yin, E. Li, C. M. Soukoulis, and H. Chen, "Full-polarization 3D metasurface cloak with preserved amplitude and phase," Adv. Mater. **28**, 6866–6871 (2016).
26. C. Huang, J. Yang, X. Wu, J. Song, M. Pu, C. Wang, and X. Luo, "Reconfigurable metasurface cloak for dynamical electromagnetic illusions," ACS Photon. **5**, 1718–1725 (2017).
27. P. A. Budni, L. A. Pomeranz, M. L. Lemons, C. A. Miller, J. R. Mosto, and E. P. Chicklis, "Efficient mid-infrared laser using 1.9-μm-pumped Ho:YAG and $ZnGeP_2$ optical parametric oscillators," J. Opt. Soc. Am. B. **17**, 723–728 (2000).
28. R. W. Waynant, I. K. Ilev, and I. Gannot, "Mid-infrared laser applications in medicine and biology," Philos. Trans. R. Soc. A **359**, 635–644 (2001).
29. T. Töpfer, K. P. Petrov, Y. Mine, D. Jundt, R. F. Curl, and F. K. Tittel, "Room-temperature mid-infrared laser sensor for trace gas detection," Appl. Opt. **36**, 8042–8049 (1997).
30. P. Werle, F. Slemr, K. Maurer, R. Kormann, R. Mucke, and B. Janker, "Near- and mid-infrared laser-optical sensors for gas analysis," Opt. Laser Eng. **37**, 101–114 (2002).
31. A. Schliesser, N. Picqué, and T. W. Hansch, "Mid-infrared frequency combs," Nat. Photonics **6**, 440–449 (2012).
32. L. H. Gabrielli, J. Cardenas, C. B. Poitras, and M. Lipson, "Silicon nanostructure cloak operating at optical frequencies," Nat. Photonics **3**, 461–463 (2009).
33. H. F. Ma, W. X. Jiang, X. M. Yang, X. Y. Zhou, and T. J. Cui, "Compact-sized and broadband carpet cloak and free-space cloak," Opt. Express **17**, 19947–19959 (2009).
34. R. Liu, C. Ji, J. J. Mock, J. Y. Chin, T. J. Cui, and D. R. Smith, "Broadband ground-plane cloak," Science **323**, 366–369 (2009).
35. V. A. Tamma, J. Blair, C. J. Summers, and W. Park, "Dispersion characteristics of silicon nanorod based carpet cloaks," Opt. Express **18**, 25746–25756 (2010).
36. J. Zhang, L. Liu, Y. Luo, S. Zhang, and N. A. Mortensen, "Homogeneous optical cloak constructed with uniform layered structures," Opt. Express **19**, 8625–8631 (2011).
37. F. Zhou, Y. Bao, W. Cao, C. T. Stuart, J. Gu, W. Zhang, and C. Sun, "Hiding a realistic object using a broadband terahertz invisibility cloak," Sci. Rep. **1**, 78 (2011).
38. B. Zhang, Y. Luo, X. Liu, and G. Barbastathis, "Macroscopic invisibility cloak for visible light," Phys. Rev. Lett. **106**, 033901 (2011).
39. M. Yin, X. Y. Tian, H. X. Han, and D. C. Li, "Free-space carpet-cloak based on gradient index photonic crystals in metamaterial regime," Appl. Phys. Lett. **100**, 124101 (2012).
40. G. Scherrer, M. Hofman, M. K. Wojtek Smigaj, T.-M. Chang, D. L. Xavier Melique, O. Vanbesien, B. Cluzel, F. D. Fornel, S. Guenneau, and B. Gralak, "Photonic crystal carpet: manipulating wave fronts in the near field at 1.55 μm," Phys. Rev. B **88**, 115110 (2013).
41. M. Kraft, Y. Luo, S. A. Maier, and J. B. Pendry, "Designing plasmonic gratings with transformation optics," Phys. Rev. X **5**, 031029 (2015).
42. M. Born and E. Wolf, *Principles of Optics*, 6th. ed. (Pergamon, 1980), pp. 109–127.
43. B. Richerzhagen, "Finite element ray tracing: a new method for ray tracing in gradient-index media," Appl. Opt. **35**, 6186–6189 (1996).
44. Z. L. Mei, J. Bai, and T. J. Cui, "Illusion devices with quasi-conformal mapping," J. Electromagn. Waves Appl. **24**, 2561–2573 (2010).
45. J. H. Lee, J. Blair, V. A. Tamma, Q. Wu, S. J. Rhee, C. J. Summers, and W. Park, "Direct visualization of optical frequency invisibility cloak based on silicon nanorod array," Opt. Express **17**, 12922–12928 (2009).
46. D. Shin, Y. Urzhumov, Y. Jung, G. Kang, S. Baek, M. Choi, H. Park, K. Kim, and D. R. Smith, "Broadband electromagnetic cloaking with smart metamaterials," Nat. Commun. **3**, 1213 (2012).
47. D. F. Edwards and E. Ochoa, "Infrared refractive index of silicon," Appl. Opt. **19**, 4130–4131 (1980).
48. J. Kischkat, S. Peters, B. Gruska, M. Semtsiv, M. Chashnikova, M. Klinkmüller, O. Fedosenko, S. Machulik, A. Aleksandrova, G. Monastyrskyi, Y. Flores, and W. T. Masselink, "Mid-infrared optical properties of thin films of aluminum oxide, titanium dioxide, silicon dioxide, aluminum nitride, and silicon nitride," Appl. Opt. **51**, 6789–6798 (2012).